Application of regression models for the estimation of the flexible-base period of pile-supported structures in continuously inhomogeneous soils *

C. Medina, G. M. Álamo, L. A. Padrón, J. J. Aznárez, O. Maeso
Instituto Universitario de Sistemas Inteligentes y Aplicaciones Numéricas en Ingeniería (SIANI) Universidad de Las Palmas de Gran Canaria
Edificio Central del Parque Científico y Tecnológico
Campus Universitario de Tafira, 35017, Las Palmas de Gran Canaria, Spain
{cristina.medina, guillermo.alamo, luis.padron, juanjose.aznarez, orlando.maeso}@ulpgc.es

19 September 2018

Abstract

Although many research efforts have focused on analyzing the effects of soil-structure interaction considering homogeneous soil profiles and relevant achievements have been made under this assumption, reality is much more complex and structures are usually founded on stratified soils. It would be really interesting to be able to continue taking advantage of the knowledge and models available for homogeneous soils by developing strategies enabling to correct their results in order to consider the actual soil stratigraphy. This paper aims at estimating the flexible-base fundamental period of slender and non-slender structures supported on several pile group configurations embedded in different Gibson soils through a substructuring model which includes soil-structure interaction effects. The foundation dynamic response is obtained through a numerical model based on the integral formulation of the elastodynamic problem and the use of Green's functions for the layered half space. The results corresponding to each one of these variable-with-depth profiles are compared to those obtained for a homogeneous soil with the same average shear wave velocity in order to assess the influence of considering the effects of soil non-homogeneity. A significant influence of the soil profile on the structural flexible-base period is observed. A polynomial regression model is applied to obtain closed-form formulas for estimating the structural flexible-base period for the different soil profiles. Moreover, these formulas can also be used for computing correction factors needed to estimate the fundamental period of structures supported on layered soils from those obtained with simplified models assuming a homogeneous soil profile.

Keywords: pile foundations, layered soil, dynamic response, soil-structure interaction, substructure model, flexible-base period, machine learning, regression model

*Draft of the paper originally published in Engineering Structures 2019; 190:76-89. https://doi.org/10.1016/j.engstruct.2019.03.112.

1 Introduction

The dynamic behaviour of pile foundations is affected by the properties of the soil in which they are embedded. Studies considering homogeneous half spaces have been conducted by numerous authors. For instance, Mamoon *et al.* [1] presented an hybrid boundary element formulation able to evaluate impedance functions of pile groups. Kaynia [2] obtained dynamic stiffnesses for several configurations of pile groups embedded in a homogeneous half space through a formulation based on Green's functions. Padrón *et al.* [3] used a boundary element - finite element coupling model to obtain dynamic impedances of single piles and several configurations of pile groups comprising inclined elements. Subsequently, the same model was applied by Medina *et al.* [4] to compute the kinematic interaction factors corresponding to several pile groups.

The impedance problem for pile foundations in non-homogeneous soils has also been addressed by several authors. For instance, Velez *et al.* [5] presented an analysis of the dynamic response of single constrained-head piles embedded in a non-homogeneous soil stratum performed by using a finite element formulation. Kaynia and Kausel [6] provided a set of representative results in terms of dynamic stiffnesses of vertical pile groups embedded in a layered half space. Rovithis *et al.* [7], Giannakou *et al.* [8] and Álamo *et al.* [9] analysed impedances of piles embedded in a soil profile whose properties vary according to a power law.

Regarding the dynamic behaviour of the superstructure, Avilés and Suárez [10] and Fu *et al.* [11] obtained the soil-structure system frequency and damping considering a foundation embedded in a soil layer over elastic bedrock concluding that the site conditions have significant influences on both parameters. Álamo *et al.* [12] studied the differences between the seismic response of real offshore wind turbines on monopiles when embedded in homogeneous or variable-with-depth soil profiles. Regarding pile supported buildings, several authors have already studied the influence of soil-structure interaction on their dynamic response considering an homogeneous soil (*e.g.* [13, 14]). However, to the best of the authors knowledge, there are no studies of this nature addressing the effects of the variability of the soil profile on the structural period.

The application of machine learning techniques to civil engineering problems has drawn a great attention from researchers and their use has significantly increased over the last decade. A recent literature review on this subject is that provided by Salehi and Burgueño [15] covering relevant studies published during the last years. Multiple linear regression (MLR) is a commonly used supervised learning technique that has been applied in previous works to structural engineering problems. Yu *et al.* [16] used MLR to estimate the contributions of parameters such as the water level, temperature and time to a dam displacement. Laory *et al.* [17] used this technique in order to predict the natural frequencies of the Tamar Suspension Bridge. Other works using this technique are those presented by Liu and Dewolf [18], Moser and Moaveni [19] or Yang *et al.* [20].

This paper aims at providing closed-form formulas to obtain the flexible-base fundamental periods of piled structures supported on variable-with-depth soil profiles. These formulas can also be used to estimate correction factors enabling to compute the flexible-base fundamental period from those corresponding to the same structure on an elastodynamic equivalent homogeneous half space. These formulas are obtained by a machine learning strategy consisting in a two-step polynomial regression model whose training and test datasets comprise results in terms of flexible-base period corresponding to slender and non-slender structures supported on several configurations of 2×2 and 3×3 vertical

pile groups. These results are computed through a procedure based on a substructuring model in the frequency domain which considers soil-structure interaction effects. An efficient numerical model based on the integral formulation of the elastic problem and specific Green's functions for the layered half space is used to compute the impedance functions corresponding to all the configurations under investigation. The influence of considering the actual variable soil-profile is assessed through comparisons against the results obtained for an elastodynamic equivalent homogeneous half space.

2 Problem definition

The influence of soil non-homogeneity on the flexible-base period of piled structures is assessed in this work through comparisons between the results obtained when considering several variable-with-depth soil profiles (see Figure 1 b) and those corresponding to the same structure when supported on an equivalent homogeneous half space (see Figure 1 c).

A three-degrees-of-freedom (3DOF) system as the one depicted in Figure 1 is used in this paper to analyse the flexible-base fundamental period of structures considering soil-foundation interaction effects. This 3DOF system is commonly used in this type of studies and may represent either one-storey structures or one mode of vibration of multi-storey buildings. It is defined by the structural horizontal deflection u, together with the foundation horizontal displacement u^c and rocking φ^c.

The structural mass m is located at the height h of the resultant of the inertia forces for the mode of vibration under study. This mass is considered to be distributed over a square area and supported by massless and axially inextensible columns. The moment of inertia of the vibrating mass is denoted by I. The structural fixed-base fundamental period is denoted by T.

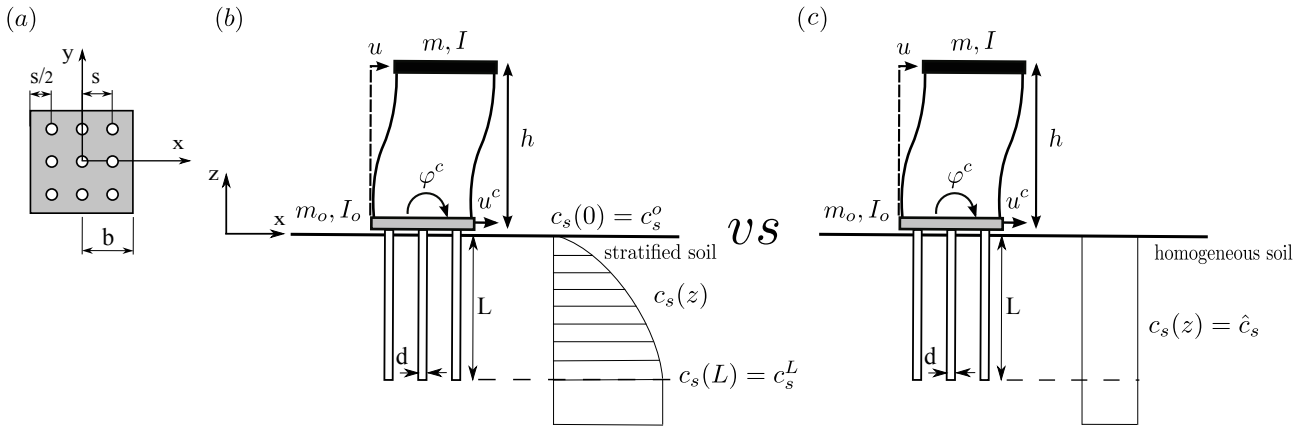

Figure 1: (a) Top view of the pile cap (3×3 pile group configuration) (b) Problem definition. Stratified soil. (c) Problem definition. Homogeneous soil.

2.1 Soil profile definition

The foundation is considered to be embedded in a viscoelastic vertically non-homogeneous half space. The study of the effects of soil non-homogeneity is addressed by considering different Gibson soil profiles whose shear wave velocity c_s varies with depth following the expression:

$$c_s(z) = c_s^L \left[q + (1-q)\frac{|z|}{L} \right]^{0.5} \qquad \text{with} \qquad q = \left(\frac{c_s^o}{c_s^L} \right)^2 \tag{1}$$

where L is the piles length, q is a dimensionless parameter that defines the soil non-homogeneity and c_s^o/c_s^L is the ratio between the shear wave velocities at the pile head and tip. The value of the shear wave velocity is kept constant for depth below the pile end (see Figure 1b). Assuming constant density ρ_s, constant Poissons ratio ν_s, and constant hysteretic damping coefficient ξ_s, the profile can also be expressed in terms of a linear Young's modulus with depth (Gibson soil [22]) as:

$$E_s(z) = \begin{cases} E_s^L \left[q + (1-q)\frac{|z|}{L} \right] & \text{if} \quad 0 \le |z| \le L \\ E_s^L & \text{if} \quad |z| > L \end{cases} \tag{2}$$

where E_s^L corresponds to the soil Young's modulus at the pile tip level.

The velocity of propagation of the shear waves in the equivalent homogeneous half space is computed through equation (3) as the average velocity of propagation of shear waves in the variable-with-depth soil profiles $\hat{c}_s$ (see Figure 1c).

$$\hat{c}_s = \frac{L}{\int_0^L \frac{dz}{c_s(z)}} \tag{3}$$

This definition of the average shear wave velocity is based on the one used by the Eurocode [23] for the clasification of the soil type and represents the shear wave velocity of an homogeneous media in which the shear wave takes the same time to travel along the pile length as in the variable profile. The other soil parameters (ρ_s, ξ_s, ν_s) of the equivalent homogeneous medium are assumed to be the same as the ones used in the variable profile. The Young's modulus for the homogeneous profile obtained from these properties will be denoted as $\hat{E}_s$.

Five different soil profiles are considered in this study. Each soil profile is defined by the ratio between the shear wave velocity at the surface and at the pile tip level (c_s^o/c_s^L), which is equal to the unit for the homogeneous soil profile. In Figure 2 the variation with depth of the shear wave velocity $c_s(z)$ as well as that of the soil Young's modulus $E_s(z)$ are represented normalized, respectively, with the average shear wave velocity $\hat{c}_s$ and the average Young's modulus $\hat{E}_s$ for each one of these soil profiles.

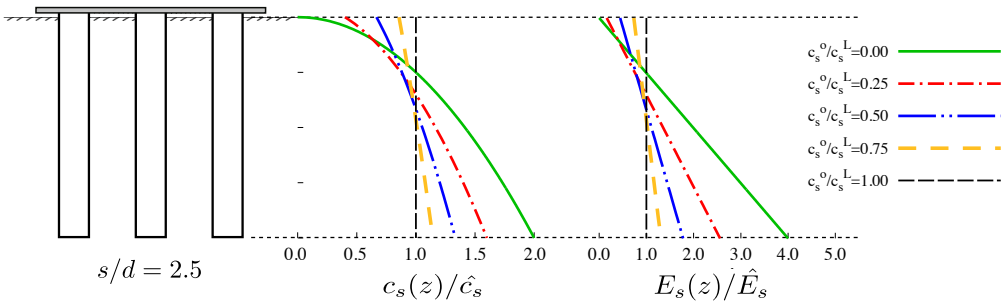

Figure 2: Soil profiles considered in this study. Evolution of the shear wave velocity $c_s/\hat{c}_s$ and soil Young modulus $E_s/\hat{E}_s$ with depth.

2.2 Configurations under study

The foundation consists of a 2×2 or 3×3 group of vertical piles with identical geometrical properties defined by its length L and diameter d. Each one of the pile group configurations considered in this study is defined by foundation halfwidth b and centre-to-centre spacing between adjacent piles s (Figure 1a). Pile heads are fixed to a rigid square cap of negligible thickness, mass m_o and moment of inertia I_o, which is considered to be free of contact with the ground surface.

In order to explore the possibility of using a machine learning technique to obtain explicit expressions for the flexible-base fundamental period of the structure, two set of pile group configurations are considered. The geometry of the different 2×2 and 3×3 pile group configurations included in the training set is defined in Figure 3. It should be noticed that the foundation halfwith b is kept constant for all the configurations under investigation. In this study the foundation embedment ratio is considered to be $L/b = 2$. The test dataset comprises results for the pile group configurations in Table 1. The dimensionless parameters corresponding to all these configurations are listed in Table 2. The definition of the set of dimensionless parameters covering the main features of SSI that has been used to characterize the system under study can be found in Table 3.

Table 1: Geometric configuration of 2×2 and 3×3 pile groups included in the test dataset.

	2×2		3×3	
L/d	11.2	22.5	10.5	24
s/d	5.6	11.25	3.5	8

Table 2: Values for the dimensionless parameters adopted for the cases under investigation

ν_p	ν_s	$E_p/\hat{E}_s$	ρ_s/ρ_p	δ	$1/\sigma$	h/b
0.2	0.4	10^3	0.7	0.15	$0 - 0.5$	$1 - 20$

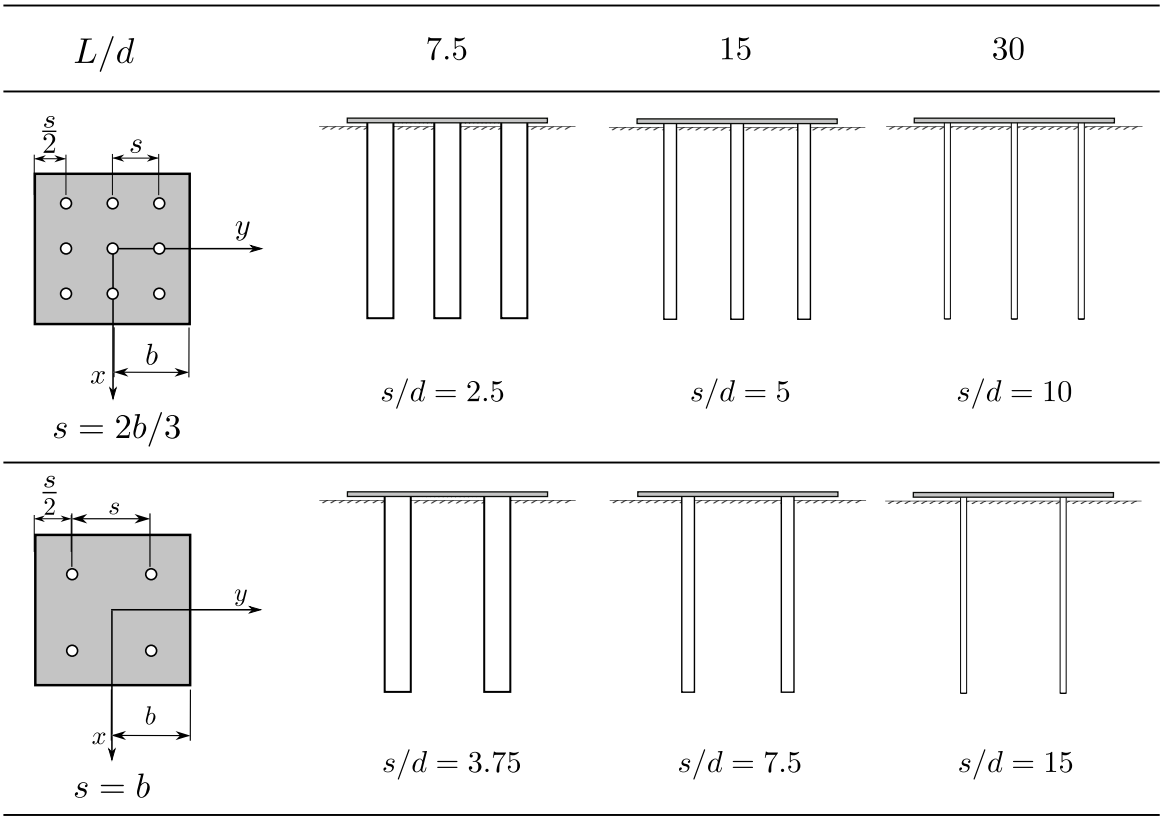

Figure 3: Geometric configuration of 2×2 and 3×3 pile groups included in the training dataset.

Table 3: Dimensionless parameters covering the main features of SSI problems [21]

ω_n/ω	dimensionless fixed-base natural frequency of the structure
h/b	structural slenderness ratio
$\delta = m/(4\rho_s b^2 h)$	mass density ratio between structure and supporting soil
$\sigma = \hat{c}_s T/h$	wave parameter measuring the soil-structure relative stiffness
ν_s	soil Poisson's ratio
ρ_s/ρ_p	soil-pile densities ratio
$E_p/\hat{E}_s$	ratio between pile Young's modulus and equivalent soil Young's modulus
s/d	pile spacing ratio
L/d	pile slenderness ratio
L/b	foundation embedment ratio

3 Methodology

3.1 Numerical model to compute pile group dynamic stiffnesses

In this paper a numerical model [9] based on the integral formulation of the reciprocity theorem in elastodynamics and the use of Green's functions for the layered half space has been used to compute the foundation impedance functions. Piles are modelled using finite elements as beams according to the Timoshenko beam theory while soil is modelled as a group of zoned homogeneous, linear, isotropic, viscoelastic layers. A sufficient number of these layers, determined from a convergence study, is used to represent the continuous non-homogeneity of the soil profile. The tractions in the pile-soil interface are considered as distributed forces acting over load lines within the soil. The variables corresponding to the piles and soil are coupled together by imposing compatibility and equilibrium conditions.

The impedance functions are written as $K_{ij} = k_{ij} + \mathrm{i}a_o c_{ij}$, where k_{ij} and c_{ij} are the frequency-dependent dynamic stiffness and damping coefficients, respectively. The dimensionless excitation frequency is defined as $a_o = \omega b/\hat{c}_s$, where ω is the excitation circular frequency.

3.2 Substructuring model to compute flexible-base fundamental periods

Once the dynamic response of the foundations has been computed, the substructuring model represented in Figure 4b allows determining the flexible-base fundamental period of the structure. The *soil-foundation* stiffness in the horizontal (k_{xx}), rocking ($k_{\theta\theta}$) and cross-coupled horizontal-rocking ($k_{x\theta}$) vibration modes, respectively, is represented by means of springs supporting the *building-cap* structure.

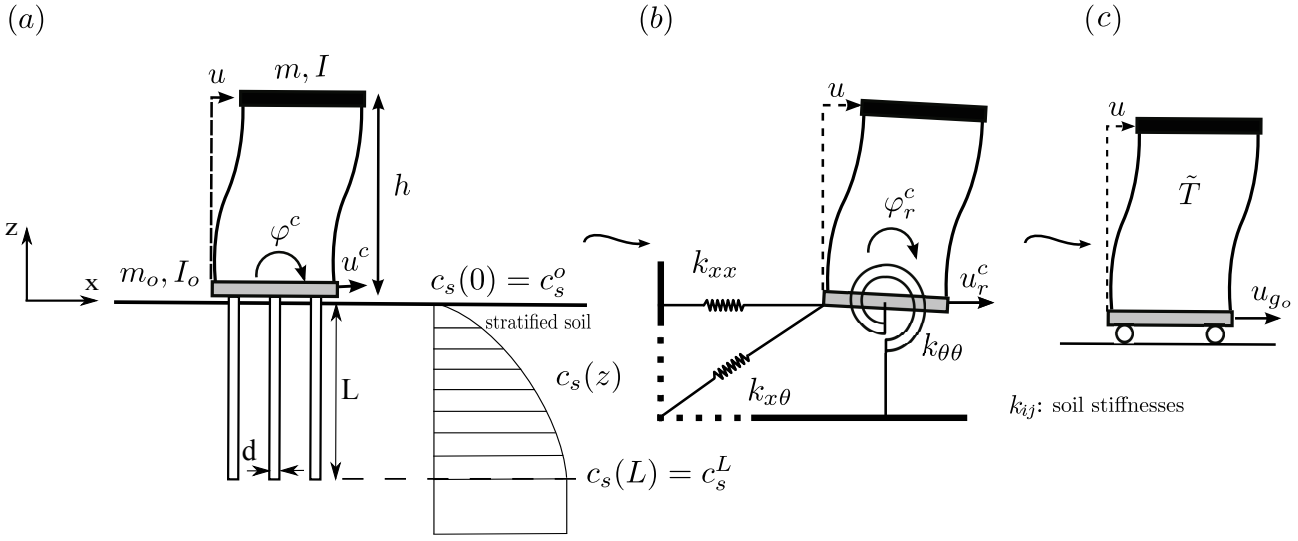

Figure 4: (a) Soil-structure-foundation system (b) substructure model of a one-storey structure and (c) single-degree-of-freedom oscillator.

Subsequently, the undamped natural period $\tilde{T}$ of an equivalent single-degree-of-freedom (SDOF)

oscillator (see Figure 4c) is estimated through a previously developed procedure [21]. The equivalence between the three- and single- degree-of-freedom systems, Figures 4b and 4c respectively, is established within the frequency range where the peak response occurs in terms of $Q = |\omega_n^2 u/(\omega^2 u_{g_o})|$, which represents the ratio of the shear force at the base of the structure to the effective earthquake force. The undamped natural period $\tilde{T}/T$ of the aforementioned equivalent SDOF system can be obtained as the value of ω_n/ω that cancels the system determinant. A detailed description of the procedure followed to obtain this value, can be found in [21].

3.3 Regression model

The results computed for the configurations of the training set are used to define a two-step polynomial regression model in order to obtain closed-form formulas for the flexible-base period of structures supported on pile groups. As shown in the figures provided in the following section, the curves obtained when representing the computed values of $\tilde{T}/T$ as a function of the inverse of the wave parameter $(1/\sigma)$ can be easily fitted using a polynomial regression model with the following form:

$$\widehat{\tilde{T}/T}\left(\frac{1}{\sigma}\right) = \beta_o + \sum_{j=1}^{3}\left(\frac{1}{\sigma}\right)^j \beta_j \tag{4}$$

where β_j are unknown coefficients and $\widehat{\tilde{T}/T}$ is the fitted ratio between the flexible-base and rigid-base periods. With a training dataset $(\sigma_1, \tilde{T}/T_1)$, ..., $(\sigma_N, \tilde{T}/T_N)$, the computation of β_j is addressed by minimizing the residual sum of squares in equation (5), where N is the number of values of σ considered. In this case, 100 values of σ between 2 and 100 have been considered ($N = 100$).

$$RSS(\beta) = \sum_{i=1}^{N}\left[(\tilde{T}/T)_i - \widehat{\tilde{T}/T}\left(\frac{1}{\sigma_i}\right)\right]^2 \tag{5}$$

The second step consists in using a multiple polynomial regression model with interaction terms, as that in equation (6), to find the best fitting polynomial able to represent the relationship between the dependent β_j and the independent variables h/b, s/d and c_s^o/c_s^L.

$$\begin{aligned}\hat{\beta}_j(h/b, s/d, c_s^o/c_s^L) = \beta_{j1} + \beta_{j2}\cdot(h/b) + \beta_{j3}\cdot(s/d) + \beta_{j4}\cdot(c_s^o/c_s^L) + \beta_{j5}\cdot(h/b)^2 + \beta_{j6}\cdot(h/b)\cdot(s/d) + \\ + \beta_{j7}\cdot(h/b)\cdot(c_s^o/c_s^L) + \beta_{j8}\cdot(s/d)^2 + \beta_{j9}\cdot(s/d)\cdot(c_s^o/c_s^L) + \beta_{j10}\cdot(c_s^o/c_s^L)^2 + \\ + \beta_{j11}\cdot(h/b)^3 + \beta_{j12}\cdot(h/b)^2\cdot(s/d) + \beta_{j13}\cdot(h/b)^2\cdot(c_s^o/c_s^L) + \beta_{j14}\cdot(h/b)\cdot(s/d)^2 + \\ + \beta_{j15}\cdot(h/b)\cdot(s/d)\cdot(c_s^o/c_s^L) + \beta_{j16}\cdot(h/b)\cdot(c_s^o/c_s^L)^2 + \beta_{j17}\cdot(s/d)^3 + \\ + \beta_{j18}\cdot(s/d)^2\cdot(c_s^o/c_s^L) + \beta_{j19}\cdot(s/d)\cdot(c_s^o/c_s^L)^2 + \beta_{j20}\cdot(c_s^o/c_s^L)^3\end{aligned} \tag{6}$$

In this case, the estimation of β_j is addressed by minimizing the residual sum of squares in equation (7).

$$RSS(\beta_j) = \sum_{i=1}^{N}\left[\beta_{j_i} - \hat{\beta}_j\left((h/b)_i, (s/d)_i, (c_s^o/c_s^L)_i\right)\right]^2 \tag{7}$$

Once these coefficients have been determined, it is possible to obtain correction factors (see equation 8) allowing the reader to estimate the effective period of structures supported on pile groups embedded in non-homogeneous soils from the values computed assuming soil homogeneity.

$$\widehat{\tilde{T}/\tilde{T}_H}\left(\frac{1}{\sigma}\right) = \frac{\hat{\beta}_o + \sum_{j=1}^{3}\left(\frac{1}{\sigma}\right)^j \hat{\beta}_j}{\hat{\beta}_o^H + \sum_{j=1}^{3}\left(\frac{1}{\sigma}\right)^j \hat{\beta}_j^H} \tag{8}$$

where $\hat{\beta}_j^H$ are the coefficients corresponding to the equivalent homogeneous soil profile.

4 Results

The substructuring methodology explained in the previous section is applied, as said in the introduction, to the investigation of the effects that the soil non-homogeneity has on the dynamic response of piled structures. In section 4.1, results are presented in terms of the relation between the flexible-base period $\tilde{T}$ and that corresponding to the fixed-base condition T. Moreover, in section 4.2, results in terms of the ratio $\tilde{T}/\tilde{T}_H$ are also provided in order to illustrate the influence of considering the variability of soil properties with depth. $\tilde{T}_H$ represents the flexible-period corresponding to an equivalent homogeneous soil profile in which the shear wave takes the same time to travel along the pile length as in the variable profile. Furthermore, in section 4.3, the regression model described in section 3.3 is used to obtain explicit mathematical expressions for the purpose of facilitating the estimation of the appropriate correction factors allowing to compute the effective period corresponding to non-homogeneous soil profiles from that obtained assuming soil homogeneity.

4.1 Flexible-base fundamental period

Figure 5 illustrates the relation $\tilde{T}/T$ between flexible-base ($\tilde{T}$) and fixed-base (T) fundamental periods obtained for slender and non-slender structures supported on different pile group configurations embedded in several soil profiles. The three top rows depict results for 2×2 pile group configurations considering three different values of the pile slenderness ratio $L/d = 7.5$, 15 and 30. Likewise, the three bottom rows provide results for 3×3 pile group configurations and the same values of L/d. Each column corresponds to different values of the structural slenderness ratio $h/b = 1$, 2, 5 and 10. In each graphical area, results corresponding to the different soil profiles under investigation ($c_s^o/c_s^L = 0$, 0.25, 0.5, 0.75 and 1 (homogeneous soil profile)) are represented in a superimposed way with different colors and line styles. The horizontal axis represents the inverse of the wave parameter $1/\sigma$. It can be seen that the ratio $\tilde{T}/T$ generally experiences a reduction as the variability of soil properties with depth increases. However, a change of trend can sometimes be observed for non-slender structures ($h/b = 1$) as the pile slenderness ratio increases, which implies softer foundations.

For the purpose of better explaining this behavior, Figure 6 presents stiffness coefficients, for the horizontal (left column), rocking (central column) and cross-coupled horizontal-rocking (right column) vibration modes, corresponding to all the configurations under study. As in Figure 5, results for the five different soil profiles are represented in a superimposed way with different colors in each graphical area. The horizontal axis represents the dimensionless excitation frequency $\omega d/\hat{c}_s$. Higher rocking

stiffnesses ($k_{\theta\theta}$) are achieved when considering the most variable soil profile ($c_s^o/c_s^L = 0$) which leads to a reduction of the effective period. However, it can be seen that pile configurations which imply softer foundations (higher pile slenderness ratio $L/d = 30$) show greater horizontal stiffness (k_{xx}) when considering homogeneous soil profile ($c_s^o/c_s^L = 1$). The extent to which these two opposing effects affect the effective period varies with the structural slenderness ratio h/b. For short and squat buildings ($h/b = 1$) the foundation horizontal stiffness has a greater influence on the system dynamic response given that in this type of structures the horizontal displacement is the controlling factor. By contrast, in the case of slender buildings the rocking stiffness takes predominance.

4.2 Correction factors

Figure 7 depicts the ratio $\tilde{T}/\tilde{T}_H$ between the system effective period obtained for each non-homogeneous soil profile ($\tilde{T}$) and that obtained for the homogeneous profile with identical $\hat{c}_s$ ($\tilde{T}_H$). These values can be interpreted as the correction factors to be applied in order to obtain the flexible-base period corresponding to an actual non-homogeneous soil from that computed assuming soil homogeneity. As in Figures 5 and 6, the three top rows depict results for 2×2 pile group configurations with three different pile slenderness ratios ($L/d = 7.5$, 15 and 30) whereas the three bottom rows correspond to 3×3 pile group configurations with the same values of L/d . Each column show results computed for a different value of the structural slenderness ratio ($h/b = 1$, 2, 5 and 10). Results for several layered soil profiles ($c_s^o/c_s^L = 0$, 0.25, 0.5 and 0.75) are represented in a superimposed way using different colours and line styles. The horizontal axis represents the inverse of the wave parameter $1/\sigma$.

It can be seen that the differences between the results obtained for the different soil profiles increase with $1/\sigma$. For structures such that $h/b = 2$, 5 and 10, the flexible-base period decreases as the variability with depth of the soil profile increases, presenting lower values compared to the case when the foundation is embedded in the homogeneous soil profile ($\tilde{T}/\tilde{T}_H < 1$). This trend is no longer seen for non-slender structures ($h/b = 1$) when considering softer configurations for the foundation ($L/d = 30$), case in which the ratio $\tilde{T}/\tilde{T}_H$ is always higher than one (*i.e.*, lowest period for homogeneous scenario). This fact is a consequence of the effect of those trends observed in the stiffness values already exposed in the previous section. It is worth mentioning that for a superstructure such that $h/b = 2$ supported on the softer configurations ($L/d = 30$), similar values are obtained for all the considered soil profiles except for that with $c_s^o/c_s^L = 0$.

4.3 Closed-form formulas

The two-step polynomial regression model described in section 3.3 is used herein in order to provide explicit mathematical expressions to enable the obtention of the appropriate correction factors allowing to compute the effective period of slender and non-slender structures supported on 2×2 or 3×3 pile groups embedded in non-homogeneous soil profiles from those obtained assuming soil homogeneity or directly from the structural fixed-base fundamental period. These expressions are valid for all the configurations whose dimensionless parameters are within the ranges considered in this study.

The model is initially fit on the training dataset considering that the structural slenderness ratio takes values such as $h/b = 1$, 1.25, 1.5, 1.75, 2, 4, 6, ..., 18, 20.

As explained in section 3, a two-steps least squares regression method is used to compute the coefficients of equation (6) which are given in Tables 4, 5 and 6, respectively, for the following ranges of the

structural slenderness ratio: $1 \leq h/b \leq 2$, $2 \leq h/b \leq 10$ and $10 \leq h/b \leq 20$. These coefficients enable, in turn, to determine the coefficients of equation (4) which is an explicit mathematical expression for the ratio $\widehat{\tilde{T}/T}$ between flexible-base and fixed-base fundamental period. Likewise, these coefficients can also be introduced in equation (8) to obtain the correction factors $\widehat{\tilde{T}/\tilde{T}_H}$.

Table 4: Coefficients of equation (6) used in turn to compute the coefficients of equation (4) defining the mathematical expression for $\widehat{\tilde{T}/T}$ in the range $1 \leq h/b \leq 2$.

	2×2				3×3			
k	β_{ok}	β_{1k}	β_{2k}	β_{3k}	β_{ok}	β_{1k}	β_{2k}	β_{3k}
1	1.00e+00	-5.23e-01	1.46e+01	-1.27e+01	1.05e+00	-2.11e+00	2.19e+01	-1.66e+01
2	1.49e-02	9.54e-02	-1.55e+01	1.58e+01	-7.15e-02	2.90e+00	-3.07e+01	2.69e+01
3	-7.62e-05	2.54e-03	6.14e-04	-4.15e-03	-3.06e-04	9.26e-03	-2.30e-02	-6.70e-03
4	-7.78e-03	6.80e-02	8.84e+00	-7.41e+00	2.47e-02	-1.08e+00	1.55e+01	-1.39e+01
5	-2.04e-02	4.07e-01	5.49e+00	-6.13e+00	2.31e-02	-1.07e+00	1.38e+01	-1.34e+01
6	3.82e-03	-1.37e-01	6.03e-01	-3.86e-01	8.97e-03	-2.84e-01	1.40e+00	-6.04e-01
7	5.24e-03	-2.68e-01	3.39e+00	-4.10e+00	-1.77e-03	7.21e-02	-1.26e+00	1.20e+00
8	-5.71e-04	1.90e-02	4.63e-03	-3.11e-02	-1.52e-03	4.62e-02	-1.14e-01	-3.34e-02
9	-1.49e-03	6.32e-02	-6.40e-01	4.98e-01	-4.94e-03	1.79e-01	-1.45e+00	1.17e+00
10	1.17e-02	-4.21e-02	-1.45e+01	1.39e+01	-2.11e-02	1.03e+00	-1.66e+01	1.52e+01
11	5.13e-03	-1.33e-01	-6.04e-01	7.27e-01	-2.03e-03	1.20e-01	-2.04e+00	2.14e+00
12	-7.74e-04	2.90e-02	-7.56e-02	5.51e-02	-1.97e-03	6.43e-02	-3.02e-01	1.71e-01
13	9.34e-04	2.70e-02	-1.26e+00	1.54e+00	2.33e-04	3.39e-02	-7.49e-01	9.45e-01
14	-3.86e-05	1.23e-03	-1.86e-02	1.16e-02	-1.44e-04	4.47e-03	-3.72e-02	1.57e-02
15	-7.33e-04	2.27e-02	1.73e-01	-1.69e-01	2.33e-04	-1.65e-02	4.22e-01	-4.21e-01
16	-2.96e-03	8.08e-03	8.07e-01	-9.49e-01	8.99e-04	-1.37e-01	2.36e+00	-2.74e+00
17	2.19e-05	-7.14e-04	7.19e-04	6.72e-04	9.59e-05	-2.89e-03	9.52e-03	1.03e-03
18	1.21e-04	-4.18e-03	-5.59e-03	9.78e-03	2.15e-04	-6.92e-03	9.37e-03	2.60e-04
19	6.71e-04	-2.75e-02	2.44e-01	-1.99e-01	1.49e-03	-5.02e-02	3.41e-01	-2.30e-01
20	-6.77e-03	1.53e-01	5.15e+00	-4.99e+00	5.07e-03	-2.37e-01	5.00e+00	-4.33e+00

4.4 Regression model accuracy

For the purpose of assessing the accuracy of the obtained model, firstly the differences between the results computed from the obtained expressions (see (4)) and those used to train the model are determined in terms of root mean square error (see equation (9)) as well as in terms of maximum relative error (see equation (10)) and shown in Table 7.

$$\mathrm{RMSE} = \sqrt{\frac{\sum_{i=1}^{N}\left(\widehat{\tilde{T}/T}(\sigma_i) - \tilde{T}/T(\sigma_i)\right)^2}{N}} \tag{9}$$

$$\mathrm{MRE} = \mathrm{Max}_{\sigma_i}\left(\frac{\widehat{\tilde{T}/T}(\sigma_i) - \tilde{T}/T(\sigma_i)}{\tilde{T}/T(\sigma_i)}\right) \tag{10}$$

Table 5: Coefficients of equation (6) used in turn to compute the coefficients of equation (4) defining the mathematical expression for $\widehat{\tilde{T}/T}$ in the range $2 \leq h/b \leq 10$.

	2×2				3×3			
k	β_{ok}	β_{1k}	β_{2k}	β_{3k}	β_{ok}	β_{1k}	β_{2k}	β_{3k}
1	9.98e-01	8.22e-02	3.40e+00	-1.71e+00	1.00e+00	-1.62e-01	3.56e+00	-1.49e+00
2	3.09e-03	-9.42e-02	-7.49e-01	7.41e-01	-1.50e-03	6.39e-02	-1.22e+00	8.52e-01
3	2.33e-05	-9.04e-04	6.18e-03	-4.87e-03	1.97e-05	-6.18e-04	3.59e-03	-2.54e-03
4	2.86e-02	-1.17e+00	5.46e+00	-4.01e+00	1.78e-02	-6.34e-01	3.60e+00	-1.89e+00
5	-2.20e-04	5.50e-03	1.25e-01	-1.16e-01	2.48e-04	-1.04e-02	1.78e-01	-1.32e-01
6	-6.26e-04	1.84e-02	1.44e-01	-1.54e-01	-8.70e-05	6.81e-04	1.56e-01	-1.31e-01
7	-4.68e-03	1.57e-01	6.29e-01	-7.20e-01	-1.73e-03	5.71e-02	3.91e-01	-3.62e-01
8	1.74e-04	-6.76e-03	4.63e-02	-3.65e-02	9.80e-05	-3.07e-03	1.80e-02	-1.28e-02
9	-5.18e-03	1.85e-01	1.89e-01	-3.59e-01	-2.84e-03	8.36e-02	5.03e-01	-6.90e-01
10	-6.01e-03	4.63e-01	-7.66e+00	6.79e+00	-1.09e-02	4.74e-01	-5.08e+00	3.46e+00
11	1.05e-05	-3.29e-04	-4.89e-03	4.58e-03	-6.73e-06	3.25e-04	-7.40e-03	5.79e-03
12	-6.17e-06	4.96e-04	-3.86e-03	3.63e-03	-1.93e-05	7.44e-04	-3.34e-03	1.83e-03
13	4.15e-05	-1.49e-04	-3.55e-02	3.45e-02	-5.98e-05	2.11e-03	-2.24e-02	1.45e-02
14	1.69e-05	-4.91e-04	-4.14e-03	4.49e-03	8.43e-06	-1.90e-04	-6.52e-03	5.83e-03
15	-1.29e-04	6.78e-03	1.40e-03	-1.60e-03	-1.01e-04	4.61e-03	1.49e-02	-1.66e-02
16	2.58e-03	-1.06e-01	-5.03e-02	1.08e-01	1.50e-03	-5.56e-02	-1.11e-02	6.17e-02
17	-1.23e-05	4.62e-04	-1.74e-03	1.16e-03	-1.14e-05	3.54e-04	2.80e-04	-7.39e-04
18	2.05e-04	-7.21e-03	-2.20e-02	2.75e-02	1.38e-04	-4.03e-03	-5.33e-02	5.94e-02
19	1.36e-03	-5.57e-02	9.42e-02	-4.98e-02	9.32e-04	-3.12e-02	1.64e-02	5.34e-02
20	-5.77e-03	1.18e-01	2.69e+00	-2.59e+00	-2.17e-04	-5.30e-02	1.77e+00	-1.37e+00

where $\widehat{\tilde{T}/T}$ represents the flexible-base period obtained from equation (4) and N is the number of values of the wave parameter (σ) considered.

Moreover, a set of results in terms $\tilde{T}/T$ obtained with the substructuring procedure described in section 3 and corresponding to configurations included in the test dataset (see Table 1) is compared against the results computed for the same configurations using equation (4) in order to determine the accuracy of the model when used to obtain interpolated curves. Soil profiles such that $c_s^o/c_s^L = 0.33$ and 0.85 are considered. Results yielding from this comparison are presented in Table 8 in terms of root mean square error and maximum relative error. In order to illustrate the accuracy of the model, some of these results are depicted in Figure 8 in terms of $\tilde{T}/T$. The left column correspond to soil profiles such that $c_s^o/c_s^L = 0.33$, whereas the right column present results for $c_s^o/c_s^L = 0.85$. The odd rows depict results for 2×2 pile group configurations with pile spacing ratios $s/d = 5.6$ and 11.25. The even rows show results for 3×3 pile group configurations with $s/d = 3.5$ and 8. Graphical areas in the first and the second row provide results for several structural slenderness ratios between 1 and 2 represented in a superimposed way using different colors. Likewise, graphical areas in the third and fourth row depict results for some values of h/b between 3 and 10. Finally, the fifth and sixth row show results for values of h/b between 15 and 20. Solid lines are used to depict the results obtained with the substructuring procedure ($\tilde{T}/T$) whereas dashed lines represent the results computed from equation (4) ($\widehat{\tilde{T}/T}$). No significant differences are found between both set of curves.

Table 6: Coefficients of equation (6) used in turn to compute the coefficients of equation (4) defining the mathematical expression for $\widehat{\tilde{T}/T}$ in the range $10 \leq h/b \leq 20$.

	2×2				3×3			
k	β_{ok}	β_{1k}	β_{2k}	β_{3k}	β_{ok}	β_{1k}	β_{2k}	β_{3k}
1	9.95e-01	4.68e-01	-1.74e+00	3.43e+00	9.91e-01	3.19e-01	-1.88e-01	6.24e-01
2	3.00e-03	-1.52e-01	9.66e-01	-8.92e-01	2.92e-03	-9.16e-02	3.94e-01	-2.06e-01
3	7.94e-05	-3.81e-03	1.91e-02	-1.73e-02	1.47e-04	-5.66e-03	1.68e-02	-6.14e-03
4	4.86e-02	-2.53e+00	8.96e+00	-8.02e+00	2.77e-02	-1.18e+00	2.05e+00	1.54e-01
5	-6.66e-05	3.72e-03	-3.24e-02	3.06e-02	-1.53e-04	4.58e-03	-2.31e-02	1.94e-02
6	-1.01e-03	3.83e-02	1.29e-02	-3.14e-02	-5.39e-04	1.71e-02	9.05e-02	-1.17e-01
7	-4.57e-03	1.81e-01	1.46e-01	-2.34e-01	-1.38e-03	3.61e-02	6.37e-01	-8.10e-01
8	5.94e-04	-2.85e-02	1.43e-01	-1.30e-01	7.30e-04	-2.82e-02	8.36e-02	-3.06e-02
9	-1.14e-02	4.79e-01	-3.83e-02	-1.48e-01	-8.27e-03	3.03e-01	5.30e-01	-7.58e-01
10	-4.77e-03	8.79e-01	-8.90e+00	8.88e+00	-1.95e-02	1.06e+00	-5.98e+00	5.29e+00
11	3.78e-07	-4.10e-05	5.34e-04	-5.25e-04	2.93e-06	-9.79e-05	6.10e-04	-6.68e-04
12	8.08e-06	-2.13e-04	-3.23e-04	5.21e-04	2.76e-06	3.90e-06	-1.27e-03	1.74e-03
13	3.05e-05	-7.41e-04	-4.41e-03	5.43e-03	2.41e-06	6.32e-04	-1.17e-02	1.62e-02
14	2.30e-05	-8.34e-04	-4.34e-04	8.93e-04	1.80e-05	-6.15e-04	-2.75e-03	3.36e-03
15	-5.63e-07	2.58e-03	-6.02e-03	7.75e-03	-1.34e-04	6.11e-03	-1.87e-02	1.80e-02
16	2.01e-03	-9.47e-02	-1.12e-03	2.76e-02	9.16e-04	-3.90e-02	-1.31e-01	1.49e-01
17	-3.44e-05	1.61e-03	-6.91e-03	6.18e-03	-6.27e-05	2.43e-03	-5.92e-03	2.01e-03
18	4.32e-04	-1.79e-02	-1.10e-02	1.77e-02	5.11e-04	-1.87e-02	-3.92e-02	5.02e-02
19	1.97e-03	-1.02e-01	1.46e-01	-1.21e-01	1.94e-03	-7.45e-02	8.00e-02	-2.58e-02
20	-5.95e-03	2.17e-02	2.84e+00	-2.97e+00	5.90e-03	-3.81e-01	2.72e+00	-2.59e+00

4.5 Use of the closed-form formulas. Numerical example

In order to illustrate the use of the formulas provided in equations (4) and (8) and for the purpose of facilitating reader comprehension, two numerical examples are addressed in this section.

4.5.1 Computing the equivalent system effective period ($\widehat{\tilde{T}/T}$)

Let's consider a structure with a slenderness ratio $h/b = 3$ supported on a 3×3 pile group configuration with a pile spacing ratio $s/d = 8$ embedded in a layered soil such that $c_s^o/c_s^L = 0.33$ and $E_p/\hat{E}_s = 10^3$ being the foundation embedment ratio $L/b = 2$. The soil-structure relative stiffness is such that $1/\sigma = 0.3$ and the structural fixed-base fundamental period is $T = 1.12$. The following values are assumed for the rest of the parameters: $\nu_p = 0.2$, $\nu_s = 0.4$, $\delta = 0.15$ and $\rho_s/\rho_p = 0.7$.

This example consists in determining the flexible-base fundamental period of the structure supported on the actual soil profile, considering its non-homogeneity ($c_s^o/c_s^L = 0.33$) and knowing its fixed-base fundamental period T. Thus, the objective is to estimate the value of the ratio $\widehat{\tilde{T}/T}$ using the formula in equation (4). In order to do so, the values of the coefficients β_i must be computed through the expression in equation (6) using the coefficients β_{ik} that can be extracted from the right side of Table 5. In this case, the obtained value is $\tilde{T} = 1.61$.

Table 7: Accuracy in terms of percentage error of the results yielding from equation (4) for the configurations in the training dataset.(RMSE: Root Mean Square Error (9); MRE: Maximum Relative Error (10)).

	RMSE		MRE	
	2×2	3×3	2×2	3×3
$1 \leq h/b \leq 2$	$1.31 \pm 1.16\%$	$0.94 \pm 0.87\%$	$1.05 \pm 0.87\%$	$1.01 \pm 0.82\%$
$2 \leq h/b \leq 10$	$1.09 \pm 0.94\%$	$0.84 \pm 0.78\%$	$2.70 \pm 2.49\%$	$1.11 \pm 1.02\%$
$10 \leq h/b \leq 20$	$1.23 \pm 1.01\%$	$0.78 \pm 0.66\%$	$4.66 \pm 4.27\%$	$2.41 \pm 2.19\%$

Table 8: Accuracy in terms of percentage error of the results yielding from equation (4) for configurations not included in the training dataset.(RMSE: Root Mean Square Error (9); MRE: Maximum Relative Error (10)).

	RMSE		MRE	
	2×2	3×3	2×2	3×3
$1 \leq h/b \leq 2$	$1.10 \pm 0.95\%$	$1.26 \pm 1.02\%$	$0.99 \pm 0.81\%$	$1.59 \pm 1.20\%$
$2 \leq h/b \leq 10$	$2.58 \pm 2.27\%$	$1.29 \pm 1.24\%$	$2.31 \pm 1.89\%$	$1.13 \pm 1.05\%$
$10 \leq h/b \leq 20$	$5.04 \pm 2.39\%$	$2.78 \pm 1.52\%$	$4.94 \pm 2.87\%$	$2.59 \pm 1.28\%$

4.5.2 Computing the correction factor ($\widehat{\tilde{T}/\tilde{T}_H}$)

This example aims at illustrating the procedure to obtain the flexible-base fundamental period $\tilde{T}$ of the structure supported on the layered soil profile defined before when knowing that corresponding to the equivalent homogeneous soil profile $\tilde{T}_H$. The usefulness of this procedure lies on the fact that it enables taking advantage of any other elaborated model assuming soil homogeneity and then correct the obtained result in order to consider the actual soil profile.

Let's consider a structure with a slenderness ratio $h/b = 4.5$ supported on a 2×2 pile group configuration with a pile spacing ratio $s/d = 6$ embedded in a layered soil such that $c_s^o/c_s^L = 0.28$ and $E_p/\hat{E}_s = 10^3$ being the foundation embedment ratio $L/b = 2$. The soil-structure relative stiffness is such that $1/\sigma = 0.25$. The following values are assumed for the rest of the parameters: $\nu_p = 0.2$, $\nu_s = 0.4$, $\delta = 0.15$ and $\rho_s/\rho_p = 0.7$. For this example, let's assume that $\tilde{T}_H = 1.85$. The ratio $\widehat{\tilde{T}/\tilde{T}_H}$ can be computed through the formula in equation (8). The coefficients β_j and β_j^H must be obtained from equation (6). In turn, as explained in the first part of this example, the β_{ik} can be extracted from the left side of Table 5 corresponding to structures such that $2 \leq h/b \leq 10$ supported on 2×2 pile group configurations. In this case, the obtained value is $\tilde{T} = 1.71$.

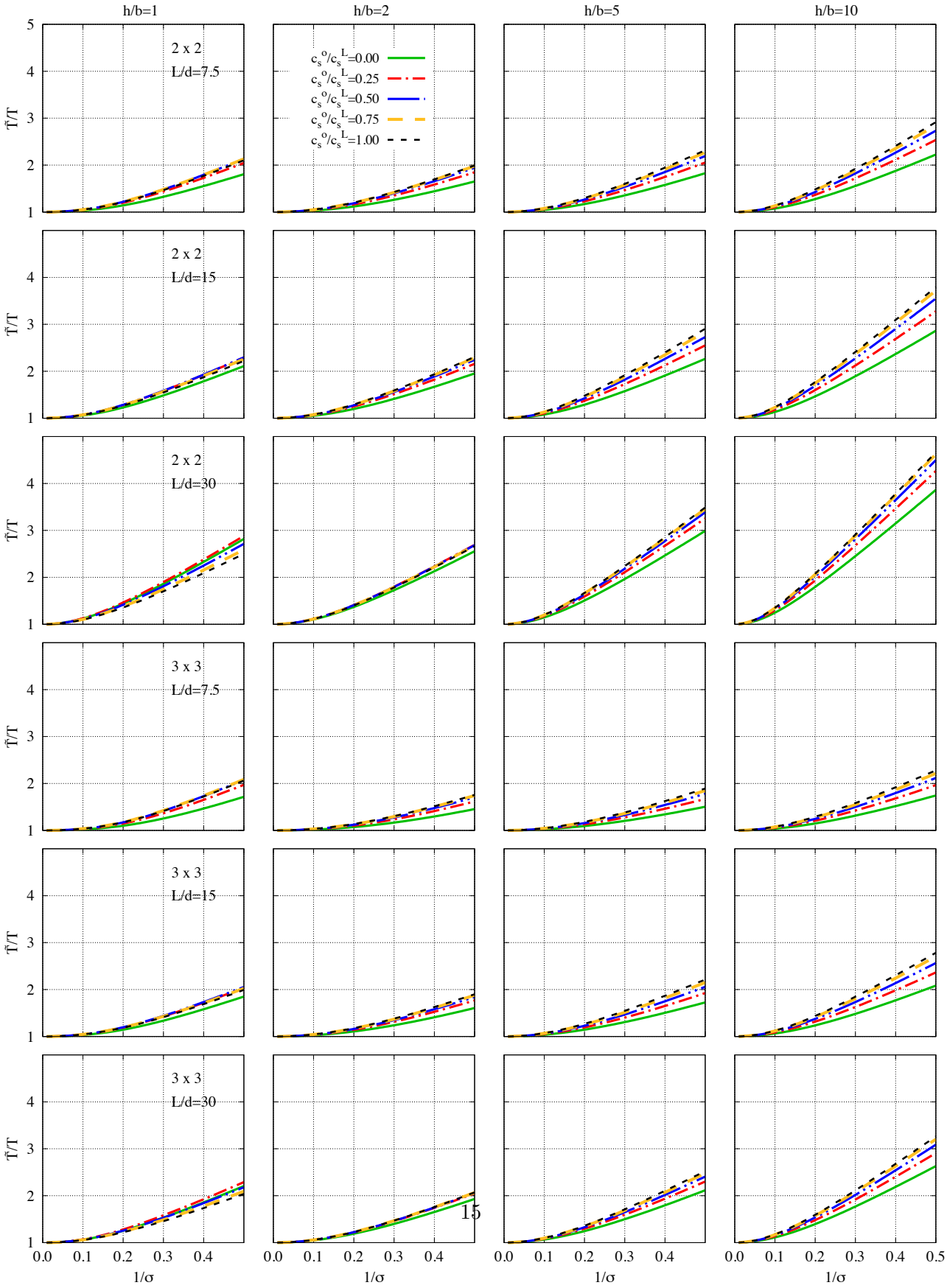

Figure 5: Ratio $\tilde{T}/T$ between flexible-base ($\tilde{T}$) and fixed-base (T) fundamental period for structures supported on 2×2 and 3×3 pile groups with $L/b = 2$ and embedded in several soil profiles ($c_s^o/c_s^L =$ 0, 0.25, 0.5, 0.75 and 1).

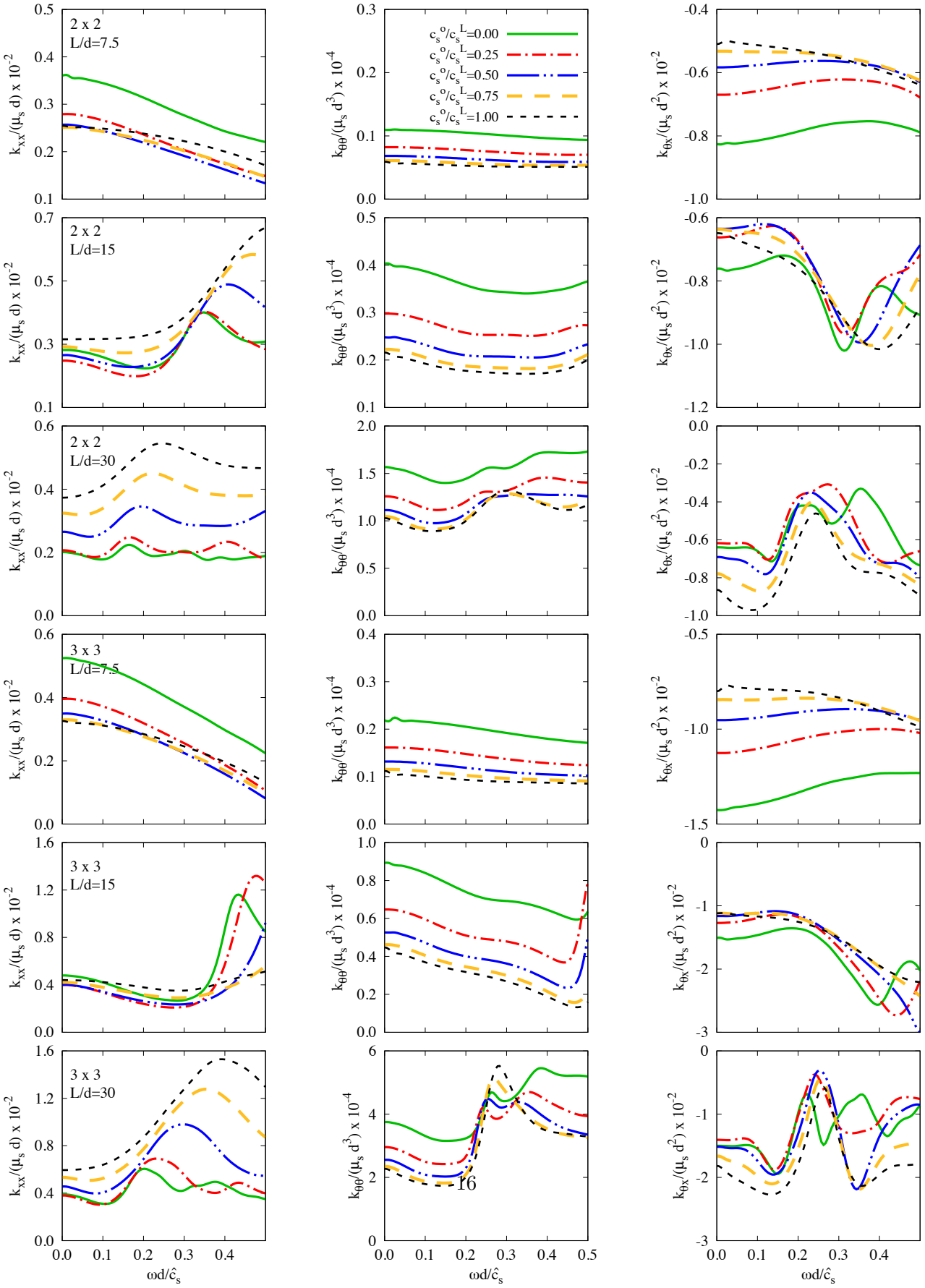

Figure 6: Dynamic stiffnesses for different 2×2 and 3×3 pile groups with $L/b = 2$ and embedded in several soil profiles ($c_s^o/c_s^L = 0$, 0.25, 0.5, 0.75 and 1).

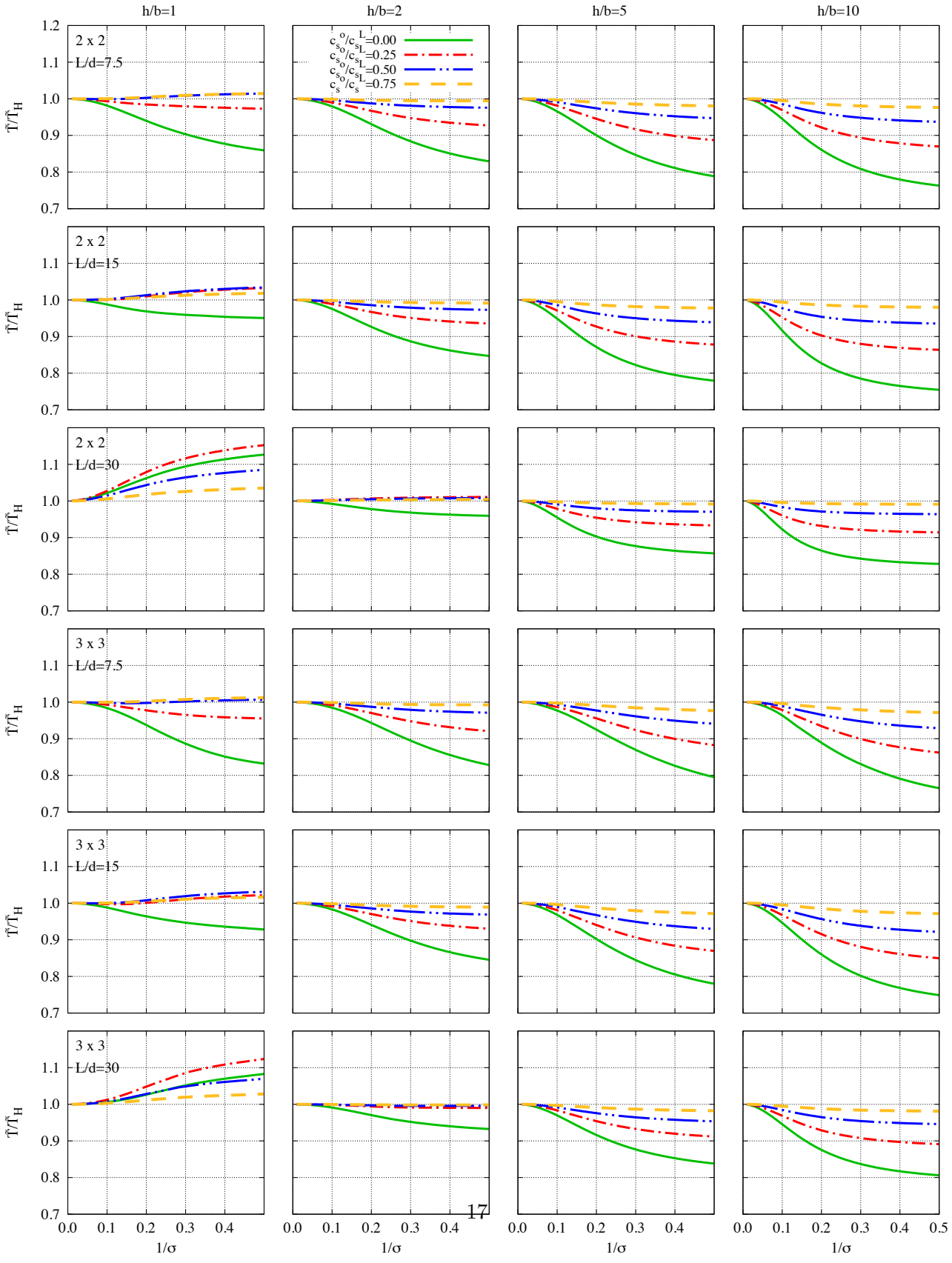

Figure 7: Ratio between the flexible-base period obtained for non-homogeneous soil profiles ($\tilde{T}$) and that corresponding to the elastodynamic equivalent homogeneous one ($\tilde{T}_H$) for different 2×2 and 3×3 pile groups with $L/b = 2$.

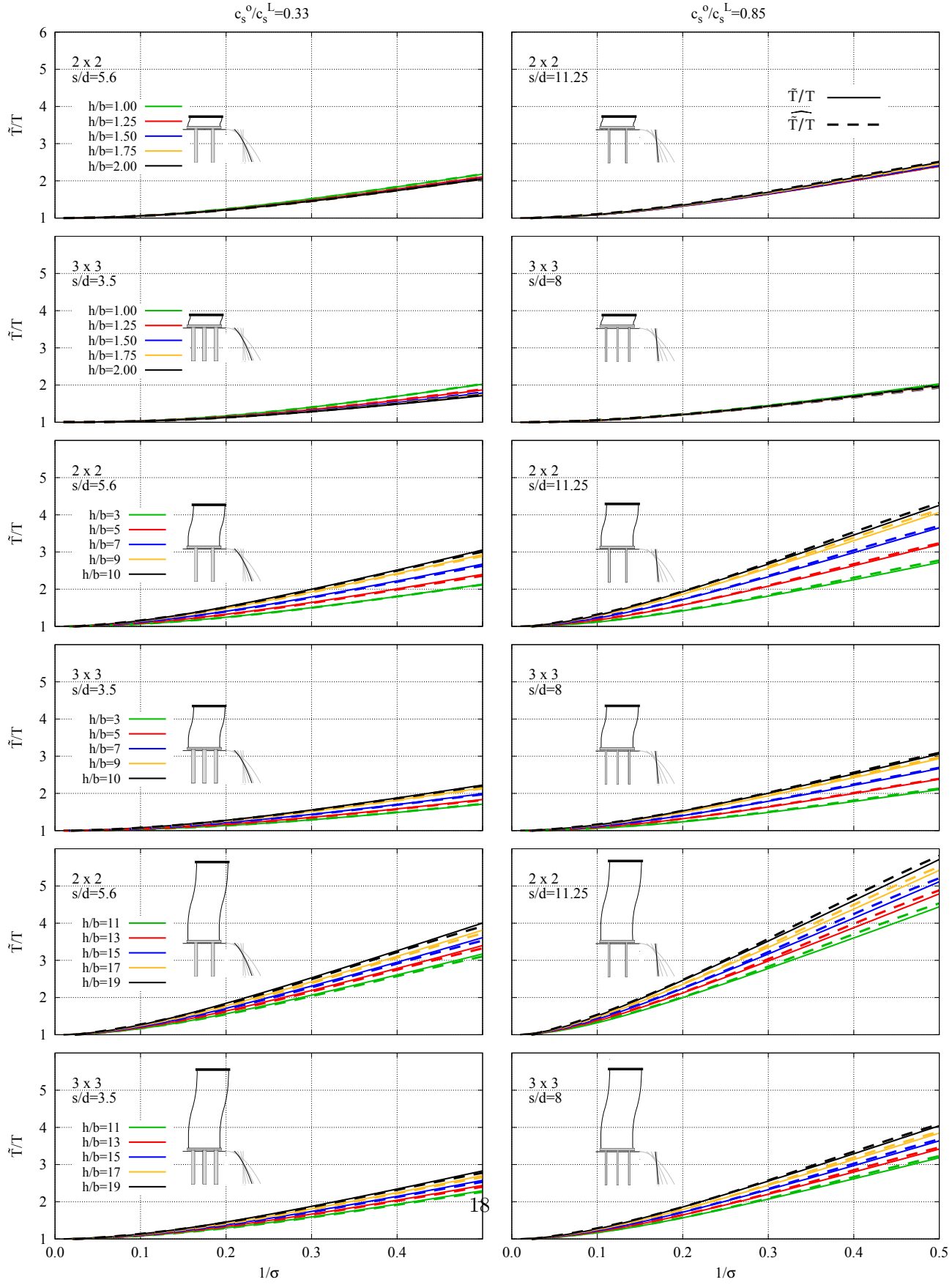

Figure 8: Ratio between the flexible-base and the fixed-base fundamental period for structures supported on 2×2 and 3×3 pile groups with $L/b = 2$ and embedded in two different non-homogeneous soil profiles ($c_s^o/c_s^L = 0.33$ and 0.85). Solid lines represent results obtained through the substructuring procedure described in section 3 ($\tilde{T}/T$) whereas dashed lines represent results computed from equation (4) ($\widehat{\tilde{T}/T}$).

5 Conclusions

An analysis to determine how the variation with depth of the shear wave velocity affects the flexible-base period of piled structures is addressed in this work. An efficient numerical model based on the integral formulation of the elastic problem and specific Green's functions for the layered half space has been used to compute the impedance functions of several pile group configurations. Then, a procedure based on a substructuring methodology is used to determine the effective period of a SDOF equivalent system. This equivalence is established in the range where the peak response occurs in terms of the maximum shear force at the base of the structure per effective earthquake force.

The flexible-base period $\tilde{T}$ of slender and non-slender structures supported by several 2×2 and 3×3 pile group configurations embedded in four different soil profiles with variable-with-depth properties as well as in an elastodynamic equivalent homogeneous soil profile is studied in this paper. It is found that $\tilde{T}$ generally decreases as the variation-with-depth of the shear wave velocity increases. This trend is clear for slender structures $h/b = 10$ but it is not so clear for non-slender structures $h/b = 1$, case in which this trend is even reversed for certain pile group configurations. This latter effect is more remarkable as the foundations stiffness decreases (*e.g.* increasing pile slenderness ratio).

This manuscript shows that a polynomial regression model can be successfully used to obtain explicit mathematical expressions for the effective period ($\tilde{T}/T$) of slender and non-slender structures supported on different 2×2 and 3×3 pile group configurations embedded in non-homogeneous soil profiles, as a function of slenderness ratio, pile spacing ratio, degree of non-homogeneity of the soil and soil-structure relative stiffness. Even though there are more complex methodologies, it has been shown that the two-step polynomial regression model used in this paper yields results accurate enough on account of the fact that $\tilde{T}/T$ increases monotonically with the inverse of the wave parameter. Evidently, this methodology could now be applied to other foundations configurations. The proposed expressions can also be used to compute correction factors allowing the reader to determine the system effective period for non-homogeneous soil profiles from the value corresponding to the assumption of soil homogeneity.

Acknowledgements

This work was supported by the Ministerio de Economía, Industria y Competitividad (MINECO) and the Agencia Estatal de Investigación (AEI) of Spain and FEDER through research projects BIA2014-57640-R and BIA2017-88770-R. G.M. Álamo is a recipient of FPU research fellowship FPU14/06115 from the Ministerio de Educación, Cultura y Deporte of Spain. The authors are grateful for this support.

References

[1] S. M. Mamoon, A. M. Kaynia, P. K. Banerjee, Frequency domain dynamic analysis of piles and pile groups, Journal or Engineering Mechanics 116(10)(1990) 2237–2257.

[2] A. M. Kaynia, Dynamic stiffness and seismic response of pile groups, Research Report R83-03, (1982) Cambridge (MA). Massachusetts Institute of Technology.

[3] L. A. Padrón, J. J. Aznárez, O. Maeso, A. Santana, Dynamic stiffness of deep foundations with inclined piles, Earthquake Engineering & Structural Dynamics 39(12) (2010) 1343–1367.

[4] C. Medina, L. A. Padrón, J.J. Aznárez, A. Santana, Kinematic interaction factors of deep foundations with inclined piles, Earthquake Engineering & Structural Dynamics 43 (2014) 2035–2050.

[5] A. Velez, G. Gazetas, R. Krishnan, Lateral dynamic response of constrained head piles. Journal of Geotechnical Engineering 109(8) (1983) 1063–1081.

[6] A. M. Kaynia, E. Kausel, Dynamics of piles and pile groups in layered soil media, Soil Dynamics and Earthquake Engineering 10(8) (1991) 386–401.

[7] E. Rovithis, G. Mylonakis, K. Pitilakis, Dynamic stiffness and kinematic response of single piles in inhomogeneous soil, Bulletin of Earthquake Engineering 11(6) (2013) 1949–1972.

[8] A. Giannakou, N. Gerolymos, G. Gazetas, On the dynamics of inclined piles. In: Proceedings of the 10th international conference on piling and deep foundations (2006) 286–295. Amsterdam (The Netherlands).

[9] G. M. Álamo, A. E. Martínez-Castro, L. A. Padrón, J. J. Aznárez, R. Gallego, O. Maeso, Efficient numerical model for the computation of impedance functions of inclined pile groups in layered soils, Engineering Structures 126 (2016) 379–390.

[10] J. Avilés, M. Suárez, Effective periods and dampings of building-foundation systems including seismic wave effects, Engineering Structures 24 (2002) 553–562.

[11] J. Fu, J. Liang, M.I. Todorovska, M. D. Trifunac, Soil-structure system frequency and damping: Estimation from eigenvalues and results for a 2D model in layered halfspace, Earthquake Engineering and Structural Dynamics 47 (2018) 2055–2075.

[12] G. M. Álamo, J. J. Aznárez, L. A. Padrón, A. E. Martínez-Castro, R. Gallego, O. Maeso, Dynamic soil-structure interaction in offshore wind turbines on monopiles in layered seabed based on real data. Ocean Engineering 156 (2018) 14–24.

[13] L. Auersch, A. Romero, P. Galvín, Respuesta dinaámica de edificaciones producida por campos de ondas incidentes considerando la interacción suelo-estructura, Revista Internacional de Meétodos Numéricos para Cálculo y Diseño en Ingeniería 30(4) (2014) 256–263.

[14] C. Medina, L. A. Padrón, J. J. Aznárez, O. Maeso, Influence of pile inclination angle on the dynamic properties and seismic response of piled structures, Soil Dynamics and Earthquake Engineering 69 (2015) 196–206.

[15] H. Salehi, R. Burgueño, Emerging artificial intelligence methods is structural engineering, Engineering Structures 171 (2018) 170–189.

[16] Y. Yu, X. Liu, E. Wang, K. Fang, L. Huang, Dam safety evaluation based on Multiple Linear Regression and numerical simulation, Rock Mechanics and Rock Engineering (2018) https://doi-org.bibproxy.ulpgc.es/10.1007/s00603-018-1435-z

[17] I. Laory, T. N. Trinh, I. F. C. Smith, J. M. W. Brownjohn, Methodologies for predicting natural frequency variation of a suspension bridge, Engineering Structures 80 (2014) 211–221.

[18] C. Liu, J.T. DeWolf, Effect of temperature on modal variability of a curved concrete bridge under ambient loads. Journal of Structural Engineering 133 (2007) 1742–1751.

[19] P. Moser,B. Moaveni, Environmental effects on the identified natural frequencies of the dowling hall footbridge. Mechanical Systems and Signal Processing 25 (2011) 2336–2357.

[20] D. Yang, D. Youliang, L. Aiqun, Structural condition assessment of long-span suspension bridges using long-term monitoring data. Earthquake Engineering and Engineering Vibration 9 (2010) 123–131.

[21] C. Medina, J. J. Aznárez, L. A. Padrón, O. Maeso, Effects of soil-structure interaction on the dynamic properties and seismic response of piled structures, Soil Dynamics and Earthquake Engineering 53 (2013) 160–175.

[22] R. E. Gibson, The analytical method in soil mechanics, Geotechnique, 24 (2) (1974) 115–140.

[23] Eurocode 8: Design of structures for earthquake resistance. Part 1:General rules, seismic actions and rules for buildings. European Committee for Standardization, Brussels. 2004.